

1 ***PDO-driven interdecadal variability of snowfall over the Karakoram and Western Himalaya***

2

3 **Authors: Priya Bharati¹, Pranab Deb¹, Kieran M. R. Hunt^{2,3}**

4

5

6 **1 CORAL, Indian Institute of Technology Kharagpur, Kharagpur, India**

7 **2 Department of Meteorology, University of Reading, Reading, UK**

8 **3 National Centre for Atmospheric Science, University of Reading, UK**

9

10

11 **Correspondence to: pranab@coral.iitkgp.ac.in**

12

13

14

15

16

17

18

19

20

21

22

23

24

25

26

27

28

29

30

31

32 **Abstract:**

33 Our study reveals that the negative phase of the Pacific Decadal Oscillation (PDO-) leads to
34 increased winter (DJF) snowfall in the Karakoram and Western Himalayas (KH) from 1940 to
35 2022. Interdecadal variations in DJF snowfall during the PDO- are attributed to deep convection
36 and adiabatic cooling near the tropopause in both the northwest Pacific and KH region.
37 Additionally, a wave-like pattern characterized by a trough (anomalous cyclone) north of KH and a
38 ridge (anomalous Tibetan Plateau anticyclone) east of KH in the upper atmosphere, along the
39 northward shift of the DJF Subtropical Jet (STJ) was observed. A strong positive correlation
40 between DJF STJ strength and DJF snowfall in KH as well as a significant negative correlation
41 between DJF STJ strength and DJF PDO, suggests a wave response over KH to the direct forcing
42 over the northwest Pacific Ocean. The intensified STJ across KH results in higher frequency of
43 Western disturbances, leading to anomalous moisture convergence and increased DJF precipitation
44 in the region during the PDO-. These findings hold significant implications for the decadal
45 predictability of winter snowfall in KH by the various phases of PDO.

46

47 **1) Introduction:**

48 Glaciers in the Karakoram and Western Himalaya (KH) exhibit unique stability compared to other
49 alpine glaciers (known as the ‘Karakoram Anomaly’; Hewitt, 2005; Kaab et al., 2012; Gardelle et
50 al., 2013; Kapnick et al., 2014; Forsythe et al., 2017; de Kok et al., 2018; Farinotti et al., 2020;
51 HIMAP, 2020). Winter snowfall plays a significant role in preserving the local snowpack and
52 sustaining the glacial mass balance at higher elevations (Tahir et al., 2011; Bolch et al., 2012;
53 Ridley et al., 2013; Cannon et al., 2015; Dimri et al., 2015), and controls almost 60% of the
54 variability in glacier mass balance in the KH region (Kumar et al., 2019). The decline in average
55 and minimum summer temperatures, along with significant increases in winter, summer, and annual
56 precipitation, have been proposed as crucial factors influencing the stable glacier budget of the KH
57 in recent decades (Archer and Fowler, 2006; Forsythe et al., 2017).

58 The KH receives around 50% of its annual precipitation as snowfall from western disturbances
59 (WDs) (Lang and Barros, 2004; Barros et al., 2006; Bookhagen and Burbank, 2010; Hunt et al.,
60 2024). Furthermore, WDs account for more than 65% of all winter snowfall and nearly 53% of total
61 winter precipitation in the KH (Javed et al., 2022). However, using a less conservative method,
62 Midhuna et al. (2020) found that WDs account for about 80% of winter precipitation in KH. WDs
63 are upper-level troughs in the subtropical westerly jet (STJ), which grow via baroclinic instability

64 (Norris et al., 2015; Cannon et al., 2017; Hunt et al., 2018). Strong WDs are associated with deep
65 uplift to the east of their centre and drive moist lower-tropospheric southwesterlies from the Arabian
66 Sea (Dimri and Dash, 2012; Hunt et al., 2018), resulting in heavy precipitation along the foothills
67 and mountains of KH region (Baudouin et al., 2020). The snowfall from WDs in the KH is heavily
68 influenced by the complex topography of the region, as well as by synoptic and mesoscale factors
69 (Cannon et al., 2015; Norris et al., 2015, 2017, 2018). Subsequent snowmelt in the following spring
70 and summer seasons and associated runoff serve as major sources of downstream river flow and
71 provide relief from drought to populations that are vulnerable to water stress (Bolch et al., 2012;
72 Hewitt et al., 2014; Rana et al., 2019; Pritchard et al., 2019).

73

74 However, the main climatic drivers affecting seasonal precipitation, and hence glacial mass balance
75 in the region are only partially understood (Cannon et al., 2015). WD activity during winter season
76 over the KH has been reported to be influenced by several global climate forcings such as North
77 Atlantic Oscillation/Arctic Oscillation (Yadav et al., 2009; Syed et al., 2010; Filippi et al., 2014;
78 Basu et al., 2017; Midhuna and Dimri, 2019; Hunt and Zaz, 2022), El Niño–Southern Oscillation
79 (ENSO) (Yadav et al., 2010; Dimri, 2013; Kar and Rana, 2014; Cannon et al., 2017; Kamil et al.,
80 2019; Rana et al., 2019; Bharati et al., 2024), Polar/Eurasian Pattern and Siberian High (Wu and
81 Wang, 2002; Cannon et al., 2014), Madden–Julian Oscillation (Barlow et al., 2005; Cannon et al.,
82 2017) and Indian Ocean Dipole (IOD) (Yadav et al., 2007; Hoell et al., 2013) on intraseasonal and
83 interannual timescales. In particular, the ENSO exerts the strongest influence on the interannual
84 variability of winter precipitation in KH (Rana et al., 2019). One of the key aspects of ENSO
85 teleconnection to Indian Himalayas is the southward shift in the latitude of the winter STJ over the
86 KH during the positive phase of ENSO (Cannon et al., 2014, 2017), which leads to heavier WD
87 precipitation as their tracks move closer to their primary moisture source, the Arabian Sea (Bharati
88 et al., 2024).

89

90 Precipitation gauges in the Himalayas are sparse and recognised as inadequate for accurately
91 measuring snowfall (Anders et al., 2006; Rana et al., 2015). While satellite records of precipitation
92 are available, they cover only a limited time frame, whereas our study requires long-term data to
93 analyse the interdecadal variability of precipitation over the KH region. We currently have an 85-
94 year-long reanalysis from ERA5, which has demonstrated a high degree of similarity in both the
95 quantity and variability of winter precipitation across all time scales when compared to observations

96 and satellite data in the KH region (Baudouin et al., 2020). The long dataset from ERA5 is
97 sufficient to examine the interdecadal variability of DJF snowfall over KH. The low-frequency
98 modes of atmospheric variability such as the Pacific Decadal Oscillation (PDO), Inter-decadal
99 Pacific Oscillation (IPO) (Mantua et al., 1998; Zhang et al., 1997; Power et al., 1999; Deser et al.,
100 2004; Dai, 2013), and the Atlantic Multi-decadal Oscillation (AMO) (Enfield et al., 2001) are
101 known to modulate the regional climate of the Northern Hemisphere over inter-decadal to multi-
102 decadal timescales. Among these, the PDO is the dominant mode of SST oscillation in the North
103 Pacific, influencing long-term precipitation patterns globally (Dettinger et al., 1998; Krishnamurthy,
104 2013, 2014; Wang et al., 2014; Dong and Dai, 2015; Yang et al., 2017; Wu and Mao, 2016; Qin et
105 al., 2017; Aggarwal et al., 2023). For example, Indian monsoon rainfall and autumn precipitation in
106 North Central China were found to have an inverse relationship with PDO (Krishnan and Sugi,
107 2003; Krishnamurthy, 2014; Qin et al., 2017). According to Aggarwal et al. (2023), the PDO has a
108 stronger positive correlation with pre-monsoon precipitation in the northwest Himalayas compared
109 to the ENSO and IOD, leading to a significant decrease in precipitation in recent decades. However,
110 there remains a significant gap in our understanding of the PDO's impact on precipitation over the
111 Himalayas during both monsoon and non-monsoon seasons.

112

113 The current study aims to address this knowledge gap by examining the modulation of the
114 interdecadal variability of winter snowfall over KH by PDO. Our study aims to understand the
115 potential influence of the PDO on the Karakoram anomaly, which deviates from the general climate
116 change patterns observed in the KH region and other mountainous areas. The main objective of this
117 study are: (1) To examine the spatial distribution of decadal snowfall in KH in different phases of
118 PDO, (2) how the PDO adjusts global circulation patterns, leading to changes in the STJ, and (3)
119 how these changes cause impact on a local scale over the KH through WDs and moisture transport.

120

121 **2) Data and Methods:**

122 **2.1 Data**

123 **2.1.1) Meteorological data**

124 The study uses meteorological data including geopotential height, zonal (u) and meridional wind (v)
125 at 200 hPa level, vertically averaged temperature from 500 to 300 hPa level, vertically integrated
126 moisture flux (VIMF), vertically integrated moisture flux convergence (VIMFC), and global sea

127 surface temperature (SST) obtained from the European Centre for Medium-Range Weather
128 Forecasts (ECMWF) ERA5 reanalysis from 1940 to 2022. The jet latitude and strength are
129 computed by 200 hPa zonal winds over the region ($50^{\circ} - 80^{\circ}\text{E}$, $10^{\circ} - 60^{\circ}\text{N}$). The jet latitude is the
130 mean of the latitudes with the largest value of u for each longitude and jet strength is the mean
131 value of u along these latitudes. ERA5 data have global coverage at hourly frequency and a
132 horizontal resolution of 0.25° .

133

134 **2.1.2) Precipitation data**

135 Precipitation in the KH is mainly observed through satellite derived and reanalysis products
136 (Bosilovich et al., 2008; Joshi et al., 2012; Ménégoz et al., 2013; Palazzi et al., 2013; Rana et al.,
137 2015; Kishore et al., 2016; Baudouin et al., 2020) due to limited and unreliable observations from
138 ground stations in this complex topographical region (Anders et al., 2006; Bookhagen and Burbank
139 2006; Strangeways, 2010; Rana et al., 2015; Dahri et al., 2018). The ERA5 reanalysis has
140 frequently been used for precipitation and snow in recent studies over the KH (Dahri et al., 2018;
141 Baudouin et al., 2020; T. Singh et al., 2021) and neighbouring mountainous areas (Hu and Yuan,
142 2020; Li et al. 2021; Dollan et al., 2014). ERA5 closely matches the most reliable gridded
143 measurements over KH in terms of amount, seasonality, and variability across all timescales during
144 winter (Baudouin et al., 2020). However, the accuracy of precipitation datasets varies depending on
145 the season in the region. We choose ERA5 due to its long period, allowing decadal-scale analysis
146 where other datasets do not.

147 To assess the performance of ERA5 precipitation, we compared the ERA5 precipitation with
148 various gridded precipitation datasets over the KH, including reanalysis datasets from ECMWF
149 ERA5-land, Modern Era Retrospective-analysis for Research, Applications version 2 (MERRA2),
150 and High Asia Refined analysis version 2 (HAR v2), as well as rain gauge, and satellite data from
151 Climate Research Unit version 7 (CRU_TS v7), Global Precipitation Climatology Center version
152 2022 (GPCC), Global Precipitation Climatology Project version 3.2 (GPCP v3.2), Asian
153 Precipitation - Highly-Resolved Observed Data Integration Towards Evaluation (APHRODITE
154 MA_v1101), CPC-Merged Analysis of Precipitation (CMAP), Tropical Rainfall Measuring Mission
155 (TRMM) Multi-satellite Precipitation Analysis (TMPA) 3B43, and Global Precipitation
156 Measurement mission-Integrated Multi-satellite Retrievals version 7 (GPM_IMERG v7).

157 We computed the linear correlation coefficient between area-averaged precipitation over the KH
158 (green box in Fig. 2a) in ERA5 and numerous other precipitation datasets. A strong correlation was

159 seen between DJF ERA5 precipitation and rain-gauge-based precipitation products, including
 160 GPCP, GPCP, and CRU, with the exception of CMAP, which exhibited a correlation coefficient of
 161 0.51 (Table 1). All reanalysis products, including ERA5 exhibit similar DJF precipitation variability
 162 as seen in observational and satellite datasets over the KH region. The variability of ERA5
 163 precipitation in the KH region aligns closely with all available gridded datasets, despite the
 164 presence of biases in ERA5 precipitation across this region. Since most of DJF precipitation in KH
 165 occurs as snowfall (fig. 1b), we utilize ERA5 snowfall data to examine the decadal variability of
 166 snowfall in the KH (73° – 78°E, 33° – 38° N).

167 **Table:1 Correlation coefficients of DJF precipitation based on monthly reanalysis, rain-gauge**
 168 **and satellite with ERA5 precipitation**

	Name	Time	Spatial resolution	Correlation with ERA5	Source
Reanalysis	ERA5-land	1980-2022	0.25°	0.99	Hersbach et al., 2018
	HAR v2	1980-2020	0.1°	0.92	Wang et al., 2021
	MERRA2	1980-2022	0.5°	0.94	Gelaro et al., 2017
Rain-gauge based	CRU_TS v7	1980-2022	0.5°	0.84	Harris et al., 2014
	GPCC v2022	1980-2020	2.5°	0.89	Schneider et al., 2018
	GPCP	1998-2022	2.5°	0.89	Adler et al., 2016
	CMAP	1980-2022	2.5°	0.51	Xie and Arkin, 1997
	APHRODITE	1998-2015	0.25°	0.67	Yatagai et al., 2012
Satellite	GPM_IMERG v07	2000-2022	0.1°	0.86	Huffman et al., 2015
	TRMM 3B43	1998-2019	0.25°	0.85	Huffman et al., 2007

--	--	--	--	--	--

169

170 **2.1.2) PDO index**

171 The PDO index from the National Oceanic and Atmospheric Administration National Climate Data
172 Center (NOAA-NDC) (<https://www.ncei.noaa.gov/access/monitoring/pdo/>) is employed to describe
173 the interdecadal variability of the Pacific Ocean over the period 1940 to 2022.

174

175 **2.1.3) Western disturbance data**

176 WD statistics are computed from the WD track catalogue described in Hunt et al., (2018) and
177 Nischal et al., (2022), which is based on ERA5 reanalysis data that is spectrally truncated to T42 to
178 remove noise and small-scale structures. The tracking algorithm detects WDs by identifying upper-
179 tropospheric regions of positive relative vorticity averaged between 450 hPa and 300 hPa, with the
180 locations of candidate WDs identified as centroids of these regions. The candidate WDs are then
181 further refined by only accepting those: 1) whose locations are linked through time to form tracks
182 that generally follow the westerly steering winds associated with the STJ, 2) that persist for at least
183 48 hours, and 3) that pass through north India (50°–77°E, 22°–42.5°N). The northern limit of this
184 box, 42.5°N, is more poleward than has been used previous studies (36.5°N). This allows us to
185 better capture WD impacts over the Karakoram.

186

187 **2.2 Methods**

188

189 **2.2.1) Lanczos filter**

190 To isolate the decadal signals, we linearly detrended all meteorological variables and the PDO index
191 for DJF. These datasets were then filtered using a 9-year running mean Lanczos filter, which is a
192 low-pass filter based on the sinc convolution (Duchon et al., 1979). The positive (negative) phase of
193 PDO is defined as years when the filtered DJF PDO index is greater than (less than) zero. We define
194 the negative epoch (PDO-) as two negative phases of PDO that occurred from 1948 to 1977 and
195 1989 to 2014, and the positive epoch (PDO+) as a positive phase of PDO that occurred from 1978
196 to 1988 (fig.1b). Also, the detrended variables are used to conduct correlation and composite

197 analyses. The Student's and Welch's t-test are used in the study to determine the statistical
198 significance of correlation and composite analyses, respectively.

199

200 2.2.2) Wavelet analysis

201 The PyCWT library (<https://pycwt.readthedocs.io/en/latest/tutorial/cwt/>) is used to calculate the
202 cross-wavelet power spectrum. This library is based on the implementation by Torrence and Compo
203 (1998). We employed the cross wavelet transform to calculate the wavelet spectrum between
204 monthly time series of the PDO index and the area averaged monthly ERA5 snowfall over the KH
205 region. The cross wavelet transform finds regions in time frequency space where the time series
206 show high common power.

207

208

209 3) Results:

210 3.1) PDO and KH winter snowfall

211 This study aims to examine the long-term variability in DJF snowfall in the KH region in relation
212 with the PDO from 1940 to 2022. There is a significant negative correlation between the lowpass-
213 filtered and detrended time series of DJF PDO and DJF snowfall in the KH (Fig 1b), with a
214 coefficient of -0.51. However, the PDO is not a single phenomenon, but rather a set of processes
215 that occur in both the tropics and the extratropics and reflects the influence of various processes
216 occurring at distinct timescales (Newman et al., 2016). More precisely, elevated sea surface
217 temperature (SST) in the eastern tropical Pacific is linked to lower SST in the central and western
218 North Pacific, while higher SST is observed in the eastern North Pacific (Deser et al. 2004;
219 Newman et al., 2016). Thus, decadal variability in the North Pacific SSTs is linked to tropical
220 Pacific decadal variability, specifically in terms of the long-lasting seasonal ENSO patterns
221 (Newman et al., 2011; Wittenberg et al. 2014) as well as the ENSO like multidecadal oscillation
222 (i.e., IPO; Zhang et al., 1997). Occasionally, the AMO may also influence multidecadal variability
223 of the PDO (Zhang and Delworth, 2007). After excluding of the influences of ENSO and IPO, the
224 correlation slightly increases to -0.53 and -0.54, and rises to -0.67 upon the elimination of the
225 AMO's impact.

226

227 The spatial structure of the correlation between PDO and KH snowfall in winter (Fig 2a) is
228 significantly negative along the western and central Himalayas and much of the southern
229 Karakoram, but positive over the Tibetan Plateau and north India. The snowfall in the KH region
230 during the boreal autumn (SON) and spring (MAM) has a strong positive correlation with the PDO
231 (not shown), whereas the summer monsoon season (JJA) displays a weak but positive correlation
232 with the PDO. The different signs of the correlation suggest that the dynamic processes driving KH
233 snowfall either vary by season, or the seasonal influence of the PDO on KH snowfall changes.

234

235 Figure 2b displays the regional distribution of the difference in detrended DJF snowfall between the
236 negative and positive phases of PDO, hereafter referred to as PDO- and PDO+, respectively. The
237 difference is significantly positive in the KH area, particularly over the southern part of the
238 Karakoram region. DJF snowfall in the KH accounts for around 80-90% of total annual snowfall
239 during the time period (not shown). During PDO+, DJF snowfall over KH is nearly 7% lower than
240 the average seasonal snowfall, while during PDO- it is about 6% higher. It indicates that the
241 difference in DJF snowfall in KH varies significantly depending on the phase of the PDO across
242 several decades.

243

244 This strong relationship between PDO and snowfall in the KH is also demonstrated through a cross-
245 wavelet frequency spectrum analysis between the unfiltered monthly time series of PDO index and
246 snowfall over the KH from 1940 to 2022 (Fig 2c). The band of strong and significant power in the
247 period of ~ 1 year in the cross-wavelet indicates that the PDO and KH snowfall both have strong
248 interannual variability. The well-known influence of ENSO on snowfall in the region (operating on
249 interannual timescales) during DJF is also slightly modulated by the low-frequency oscillation of
250 PDO. Another band of significant power exists in the 6-15 year range, indicating a high decadal
251 scale correlation between these two time series. The significant power in the 6-15-year range
252 occurred between 1940 and 1970 and again from 1998 to 2015, coinciding with the negative phases
253 of the PDO. An insignificant weak power appeared within the same range from 1971 to 1988,
254 coinciding with the positive phase of the PDO. A long band of strong power exists throughout the
255 16–20-year range, observed from 1950 to 1990, while a weaker power is shown from 2000 to 2022.
256 This indicates that the low-frequency variability of KH snowfall is influenced by decadal
257 oscillations over various time scales, while the interdecadal variability of KH snowfall is found to
258 influenced by the phase of the PDO.

259 **3.2) Sea Surface temperature (SST) variability during DJF**

260 Figure 3a illustrates the well-known positive (or warm) phase of the PDO over the North Pacific,
261 shown as a correlation between lowpass filtered and detrended sea surface temperature (SST) and
262 PDO index during DJF. The correlation pattern also reveals a strong El-Nino like pattern in the
263 eastern equatorial-tropical Pacific Ocean. For comparison, the correlation pattern between the DJF
264 SST anomalies and the DJF snowfall anomalies in the KH region is shown in Fig 3b. This
265 correlation strongly resembles the negative (or cool) phase of the PDO over the North Pacific
266 Ocean. It is characterised by positive SST anomalies in the northwest Pacific and negative SST
267 anomalies in the northeast Pacific. Additionally, there are negative SST correlations in the tropical
268 eastern Pacific region and eastern Indian Ocean adjacent to Western Australia, while positive
269 correlations are observed in the southwest Indian Ocean and across the northwest Atlantic Ocean.
270 The correlation pattern in the southern Indian Ocean reveals the subtropical Indian Ocean Dipole
271 signature (positive phase) (Behera & Yamagata, 2001; Yamagami & Tozuka, 2014).

272

273 **3.3) Upper atmosphere circulation response with PDO and snowfall**

274 To understand the anomalous atmospheric circulations that connect the PDO with anomalous DJF
275 snowfall in the KH region, we computed the correlation of 200 hPa geopotential height with both
276 the DJF PDO index (Fig 4a) and DJF snowfall (Fig 4b). The correlation pattern between the PDO
277 and upper-level geopotential height shows a prominent upper-level trough over east China, Japan
278 and the northwest Pacific, which is known as East Asian trough (EAT; Qin et al., 2018; Yin and
279 Zhang, 2021). In contrast, the correlation pattern over the Caspian Sea, KH, and Lake Baikal region
280 is associated with positive geopotential height anomalies. The EAT is a well-known upper
281 atmospheric response to the positive phase of PDO to the East Asia-North Pacific region during the
282 Northern Hemisphere winter (Newman et al, 2016; Qin et al., 2018; Yin and Zhang, 2021). The
283 intensity of the EAT is strongly linked to the strength of the winter monsoon in East Asia and the tilt
284 in the EAT axis is connected to midlatitude baroclinic processes, such as the eddy-driven jet or WD
285 tracks over the East Asia-North Pacific region (Wang et al., 2009). Therefore, changes in location
286 and intensity of the EAT can lead to, or otherwise indicate, regional climate anomalies, such as
287 temperature in the upper troposphere which subsequently influence DJF precipitation in East Asia
288 as well as the KH during the positive phase of the PDO.

289 These patterns change sign during negative phases of PDO, when KH snowfall is enhanced,
290 implying an anomalous upper-level trough to the west of the Karakoram, consistent with increased

291 WD frequency or intensity. The correlation between upper-level geopotential height and snowfall
292 has a similar pattern to the PDO-geopotential correlation, but as expected, with reversed sign. The
293 correlation pattern exhibits a strong ridge (or a weakened EAT) over the northwest Pacific and
294 Japan characterised by the significant positive geopotential height anomalies. The negative
295 correlation to the west of the KH area shows a trough, which is stronger than the positive
296 correlation between PDO and geopotential height, indicating the linkage of seasonal snowfall to the
297 passage of WDs is stronger than the link between the PDO and WDs. Both, however, are important.
298 The appearance of the anomalous trough in both pairs of correlations implies that the PDO may
299 affect KH snowfall by somehow modulating WD activity. Therefore, it is essential to understand
300 how decadal fluctuations in DJF snowfall in the KH are driven by WDs and how the PDO
301 influences WD behaviour. This can be accomplished by investigating the DJF STJ, followed by a
302 detailed investigation of the WDs.

303

304 **3.4) Modulation of WD and Subtropical Westerly Jet by the PDO**

305 To further illustrate the above relationship between PDO and DJF snowfall in KH, we examine the
306 composite differences in 200 hPa wind, geopotential height, and temperature (Fig. 5) between PDO-
307 and PDO+. Figure 5a displays the difference in 200 hPa circulation over East Asia, Arabian
308 Peninsula and northwest Pacific region. During the PDO-, there is a large negative geopotential
309 height anomaly to the north of KH region, which extends from the Caspian Sea-Arabian Peninsula
310 to KH. Strong westerlies are observed to the south of this trough with a stronger STJ prevailing
311 across KH during the PDO-. An anomalous trough in the upper atmosphere is indicative of
312 increased WD frequency (or intensity) and the frequency of WDs is strongly affected by variations
313 in both the latitude and intensity of the STJ (Dimri et al., 2015; Hunt et al., 2017, 2018) over South
314 Asia. Therefore, we now focus on understanding the relationship between the PDO and the STJ.

315

316 Upper-level jets are thermal wind responses to upper-level meridional temperature gradients. In Fig
317 5b, we show the difference in mid-to-upper (from 500 hPa to 300 hPa) tropospheric temperature
318 between PDO- and PDO+. A quadrupole in the upper air temperature gradient is present across the
319 KH, Tibetan Plateau (TP) and the northwest Pacific region during PDO-. Over the Pacific, this is
320 effectively a direct response to the anomalous surface heating provided by the PDO. Anomalous
321 warm SSTs over the northwest Pacific lead to adiabatic cooling near the tropopause, which results
322 in deep convection over the Maritime Continent during the PDO- (e.g., Wang et al., 2016).

323 Upstream, over continental Asia, the relationship is more complicated and is probably a wave
324 response to the direct forcing over the ocean. Therefore, a strongly enhanced meridional
325 temperature gradient over the KH and TP, leading to a stronger and more meridionally-locked STJ.

326

327 Figure 5c displays the lowpass filtered time series of latitude and strength of the DJF STJ. During
328 the PDO-, the STJ tends to sit slightly further north but is also substantially stronger. The
329 correlation of the time series of the strength of DJF STJ with DJF PDO is significantly negative (-
330 0.22), and the correlation between DJF STJ strength and DJF snowfall in KH is strong positive
331 (0.51). The positive (negative) phase of the PDO enhances the movement of the STJ towards the
332 south (north) through a response to the decreased (increased) SST over the northwest Pacific and
333 modulates the cyclonic (anticyclonic) circulation over the northwest Pacific and adjacent maritime
334 continents (Matsumura & Horinouchi, 2016). During PDO-, we observed a quadrupole in the
335 anomalous upper-level temperature gradient (Fig. 5b), resulting in a negative anomaly in the
336 temperature gradient and an anticyclonic circulation (Fig. 5a) over the TP. Thus, by modulating the
337 STJ, the negative phase of the PDO leads to more frequent (more intense) WDs at slightly higher
338 latitudes than usual (e.g. into the Karakoram, where the signal is the strongest).

339

340 The presence of a stronger STJ along with a wave-like pattern of trough (anomalous cyclone) over
341 the northern region of KH, and a ridge (anomalous TP anticyclone) in the upper atmosphere,
342 increases the occurrence of WDs over KH during the PDO-. After examining the impact of the PDO
343 on the STJ, we now quantify its influence on WDs directly. Maps of the difference in the frequency
344 of DJF WDs between PDO- and PDO+ (Fig 6a) indicate that WDs are more frequent (with a 9%
345 higher frequency) over the KH region during PDO- compared to PDO+. Also, the frequency of
346 WDs is found to be reduced by around 3% in both the northern and southern regions of the KH
347 during PDO- compared to PDO+. These WDs are observed to be more intense in the vicinity of the
348 Caspian Sea and north of the KH during PDO- rather than PDO+ (not shown).

349

350 **3.5) Atmospheric-ocean response of PDO on moisture transport in KH**

351 Increased frequency and intensity of WDs have a significant impact on precipitation in the KH and
352 surrounding region because they govern southwesterly moisture transport from the Arabian Sea
353 (Baudouin et al., 2021; Hunt and Dimri 2021). The composite difference of DJF VIMF and VIMFC

354 between PDO- and PDO+ is now examined to determine the response of moisture transport to the
355 PDO and its subsequent effect on the KH (Fig. 6b). The average difference of VIMFC between
356 PDO- and PDO+ is about $0.8 \times 10^{-5} \text{ kg m}^{-2} \text{ s}^{-1}$ within KH region. An advection of moisture from the
357 Black Sea, Red Sea, and eastern Mediterranean Sea through the Arabian Peninsula/Arabian Sea
358 towards the KH in westerly fashion is observed. The precipitation associated with WDs is mostly
359 determined by their intensity and proximity to the Arabian Sea (Baudouin et al., 2020). The
360 variations in the moisture transport across the Arabian Peninsula/Arabian Sea are not directly linked
361 to changes in VIMF over the northwest Pacific, but the presence of more WDs south of the strong
362 DJF STJ over KH clearly result in greater moisture transport towards KH during PDO-. Hence, the
363 anomalous moisture transport nearly perpendicular to KH, results in increased moisture flux
364 convergence about 16% greater during the PDO- compared to the PDO+ and leads to greater
365 precipitation in the region during PDO-.

366

367 **4) Conclusion and Discussion:**

368 The recent impacts of climate change over the KH, particularly in mean and extreme winter
369 precipitation, have been largely attributed largely to anthropogenic forcing, such as greenhouse
370 gases, aerosols, and changes in land use. However, these changes cannot be solely explained by
371 natural forcing (Krishnan et al., 2018). Oceanic conditions, especially changes in SSTs over the
372 equatorial-tropical Pacific and north Pacific, play an important role in driving interdecadal
373 variability in atmospheric circulation and hence winter precipitation over the KH.

374

375 DJF snowfall in the KH accounts for around 80-90% of total annual snowfall during the time
376 period, hence a 15% difference in DJF snowfall can have a significant influence on agriculture in
377 this region, especially since most of the rivers in this region, such as tributaries of Indus, Tarim and
378 Ganges are partially fed by snowmelt in the spring and later seasons (Armstrong et al., 2018).
379 Understanding the interdecadal variability and its relationship with the PDO is important for
380 understanding the long-term climate of the KH. We have analysed the long-term variability in
381 winter snowfall over the KH due to PDO by using ERA5 reanalysis data from 1940 to 2022. We
382 found that a strong negative correlation of -0.51 between the PDO and DJF snowfall in the KH.
383 Mean KH snowfall during DJF is approximately 6% greater than the DJF seasonal average during
384 PDO-, and 7% lower during PDO+.

385

386 PDO associated anomalous warming of SST in the northwest Pacific modulates the snowfall in the
387 KH via changes in upper-level temperatures over the Pacific and Asia. The warm SSTs lead to
388 increased deep convection and subsequent upper-tropospheric adiabatic cooling over the Pacific.
389 During PDO-, the anomalous heating of the tropospheric column over North Pacific leads to a wave
390 like pattern with an upper-level trough over the north of KH and upper-level ridge over the Tibetan
391 Plateau. This results in a stronger STJ to the west of, and over, the KH, before it is deflected
392 northwards over the Tibetan Plateau. There is a strong positive correlation between the strength of
393 DJF STJ and DJF snowfall in KH, with a correlation coefficient of 0.51, and a significant negative
394 correlation between the strength of STJ and PDO, with a correlation coefficient of -0.22 during DJF
395 at decadal scale. These results indicate a wave response over KH to the direct forcing of the north
396 Pacific Ocean.

397 These anomalous jet conditions over KH are linked to a higher occurrence of WDs across the
398 region. Using a track catalogue, we found that WDs are 9% more frequent across the KH and drop
399 by approximately 3% in both the northern and southern regions of the KH during PDO- compared
400 to PDO+. However, the WDs are found to be more intense in the vicinity of the Caspian Sea and
401 north of the KH during PDO- rather than PDO+, which is not shown in this study. This increase in
402 WD frequency results in anomalous moisture transport from the Arabian Sea, Black Sea, Red Sea,
403 and eastern Mediterranean Sea towards the KH. The moisture transport is almost perpendicular to
404 the orography of the KH, leading to a strong moisture convergence about 16% greater during the
405 PDO- compared to the PDO+ and thus increased DJF precipitation in the region during the negative
406 phases of the PDO.

407 Our findings highlight the importance of considering interdecadal variability when trying to
408 quantify the effects of anthropogenic climate change in the KH. The recent PDO- has led to
409 increased WD activity, and hence increased winter snowfall over this region, and may be masking
410 the effects of climate change. More research is needed to disentangle climate change from the
411 effects of interdecadal variability over this vulnerable region, so that policymakers can be better
412 informed. The uncertainty in the snowfall and precipitation datasets, along with the limitations of
413 the short timeseries available from reanalysis for examining decadal oscillations, are insufficient to
414 demonstrate such studies. Future long-term climate simulations could be used for subsequent work
415 if the models accurately represent the interaction between the PDO and snowfall/precipitation in
416 this region.

417

418 **5) List of figures:**

419

420

421

422

423

424

425

426

427

428

429

430

431

432

433

434

435

436

437

438

439

440

441

442

443

444

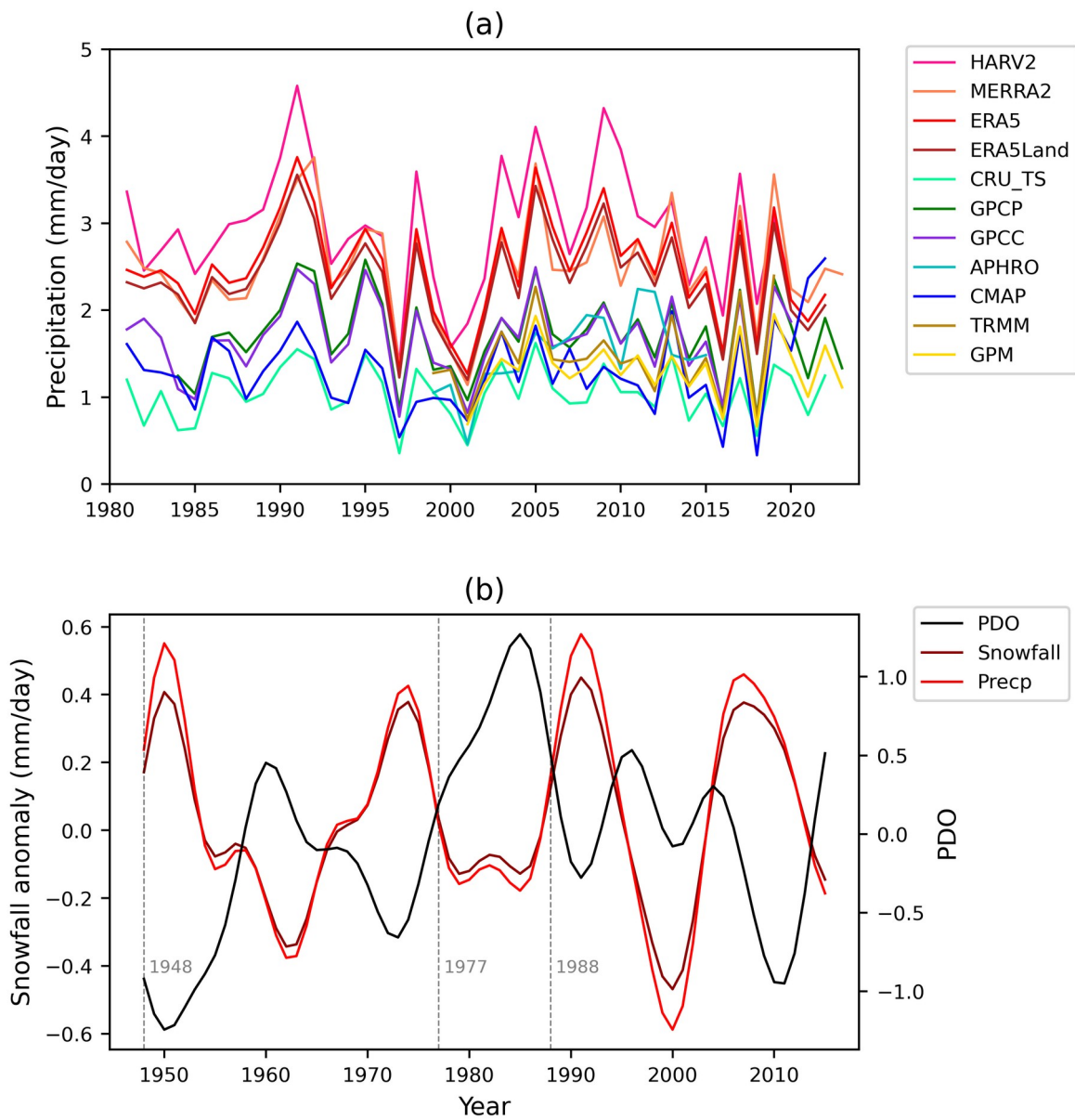
445

446

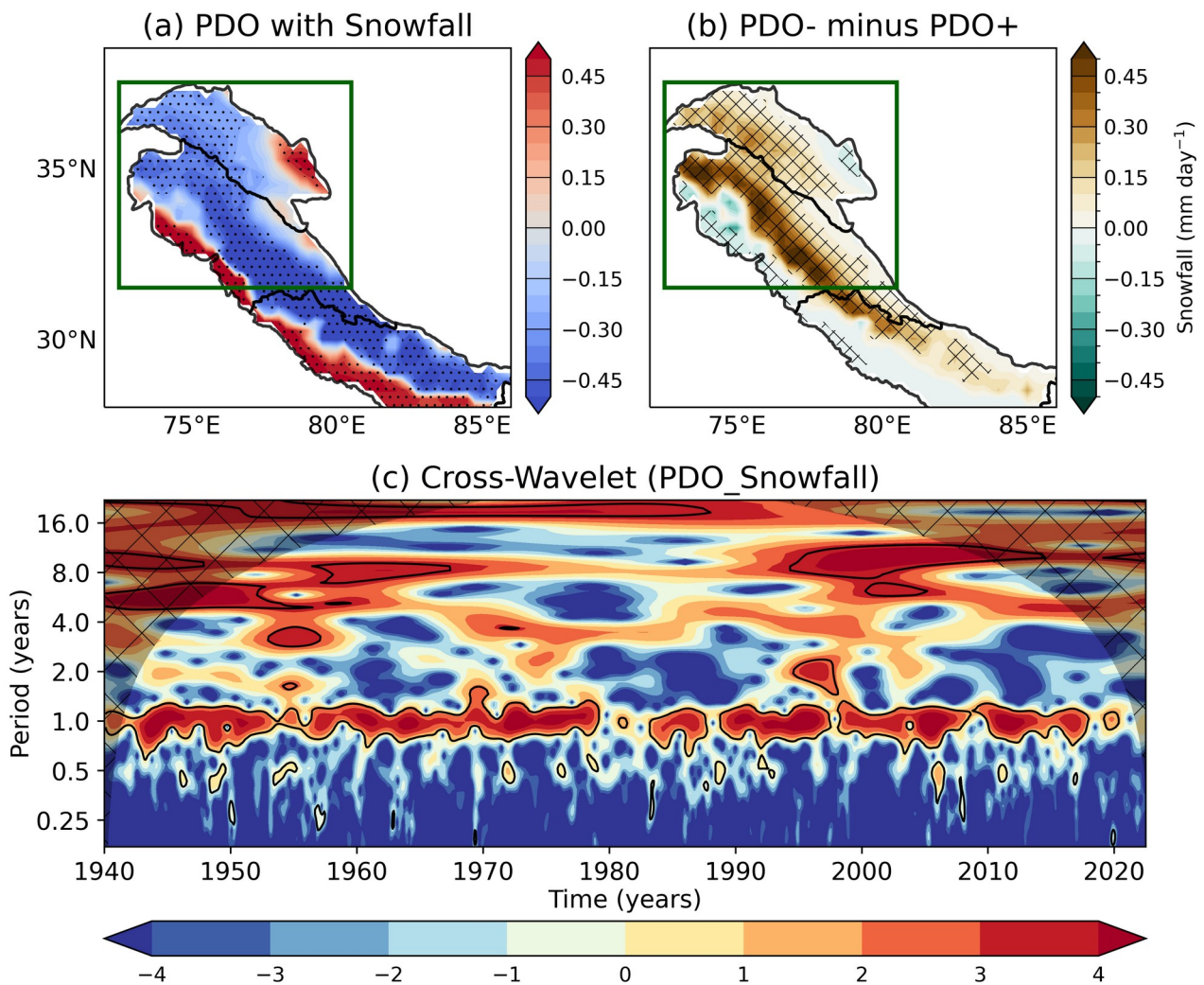
447

448

449



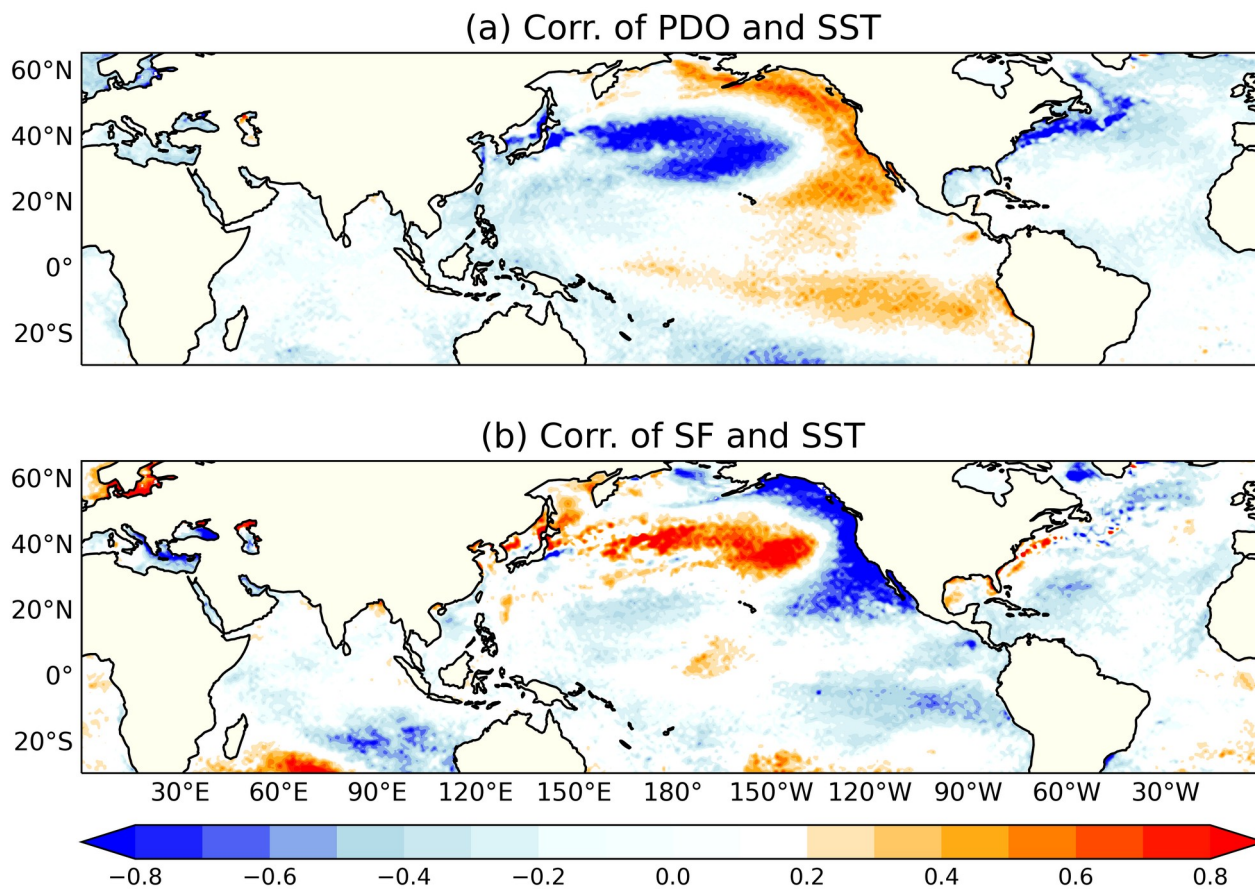
443 **Figure 1: (a) Seasonal variability of DJF precipitation in KH (green rectangle in fig.2; 73° –**
444 **78° E, 33° – 38° N) from ERA5, ERA5-land, MERRA2, HARv2, CRU_TS, GPCP, GPCP, and**
445 **CMAP during the period from 1980 to 2020, APHRODITE from 1998 to 2015, TRMM from**
446 **1998 to 2019, and GPM from 2000 to 2023. (b) Time series of 9-year filtered DJF PDO index**
447 **and area-averaged DJF ERA5 snowfall (and precipitation) anomalies over KH from 1940 to**
448 **2022. The vertical grey lines represent phase transitions of PDO.**



451 **Figure 2: (a) Spatial map of correlation between the 9-year filtered PDO index and the**
 452 **snowfall (mm) over KH during DJF, and (b) composite difference of DJF snowfall (mm)**
 453 **between negative and positive epoch of PDO, (c) cross-wavelet of DJF snowfall (mm) over KH**
 454 **and DJF PDO index from 1940 to 2022. Traditional boundaries of Karakoram-Western and**
 455 **Central Himalayan regions are marked by thick black lines in (a) and (b). Stippling in (a) and**
 456 **(b) denotes regions where the correlation and composite differences are significant at a 95%**
 457 **confidence level, as determined by the two-tailed Student's t-test and Welch's t-test,**
 458 **respectively. Black line contours on the power spectra in (c) indicate where the spectral power**
 459 **of the cross-wavelet is significantly greater than zero at a 95% confidence level.**

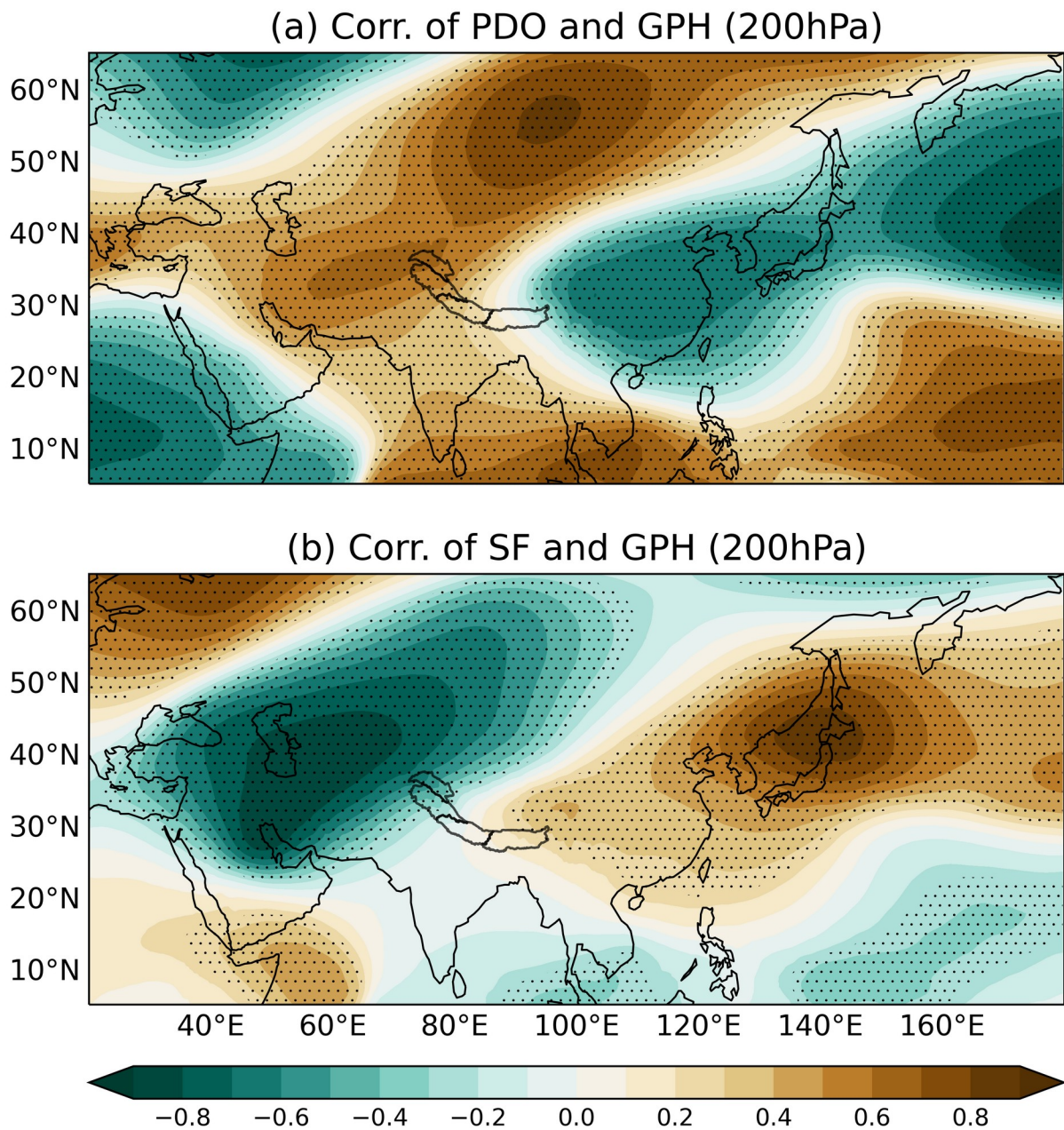
460
 461
 462
 463

464
465
466
467



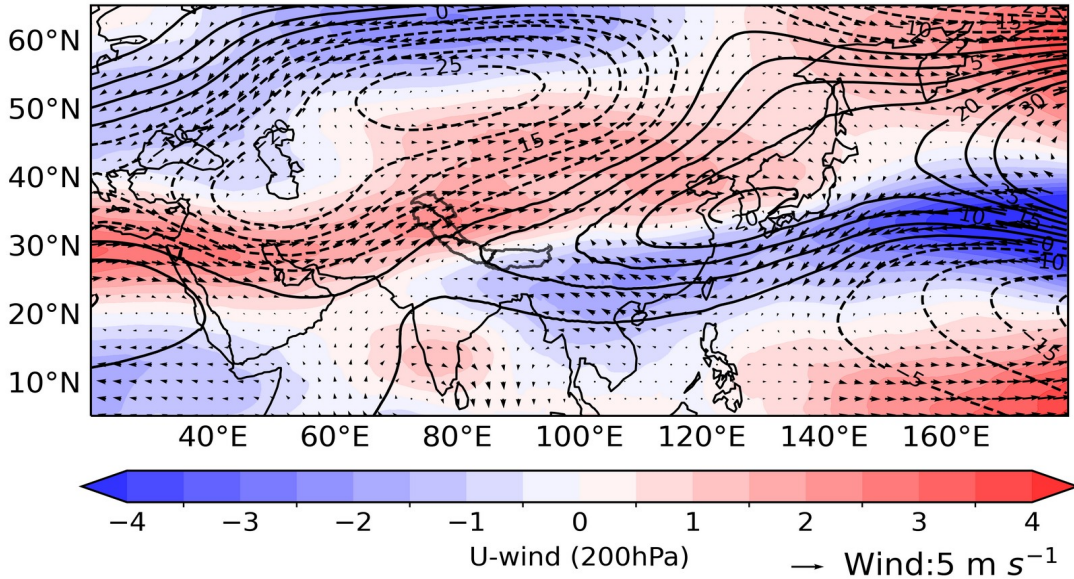
468 **Figure 3: Spatial map of correlation of the 9-year filtered (a) DJF PDO index, and (b) area**
469 **averaged DJF snowfall over the green box (fig.2) with 9-year filtered DJF sea surface**
470 **temperature from 1940 to 2022. The correlations patterns are statistically significant at the**
471 **95% confidence level, as determined by the two tailed student's t-test.**

472
473
474
475
476
477
478
479

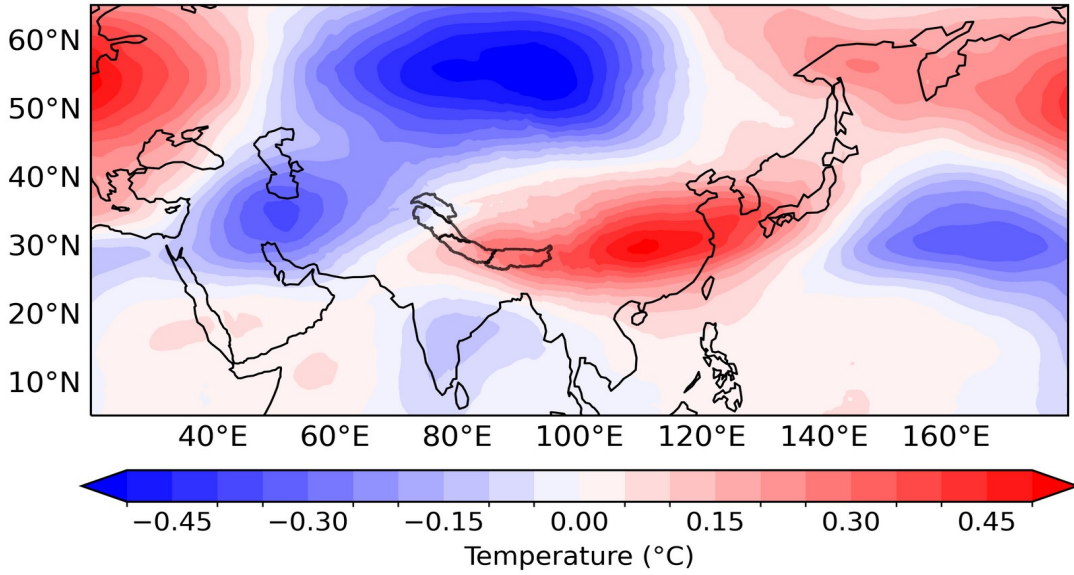


482 **Figure 4: Spatial map of correlation of the 9-year filtered (a) DJF PDO index, and (b) area**
 483 **averaged DJF snowfall (mm) over the green box (fig.2) with 9-year filtered DJF geopotential**
 484 **height at 200hPa (m) from 1940 to 2022. Stippling in (a) and (b) indicate where the**
 485 **correlations are significant at a 95% confidence level, as determined by the two tailed**
 486 **student's t-test.**

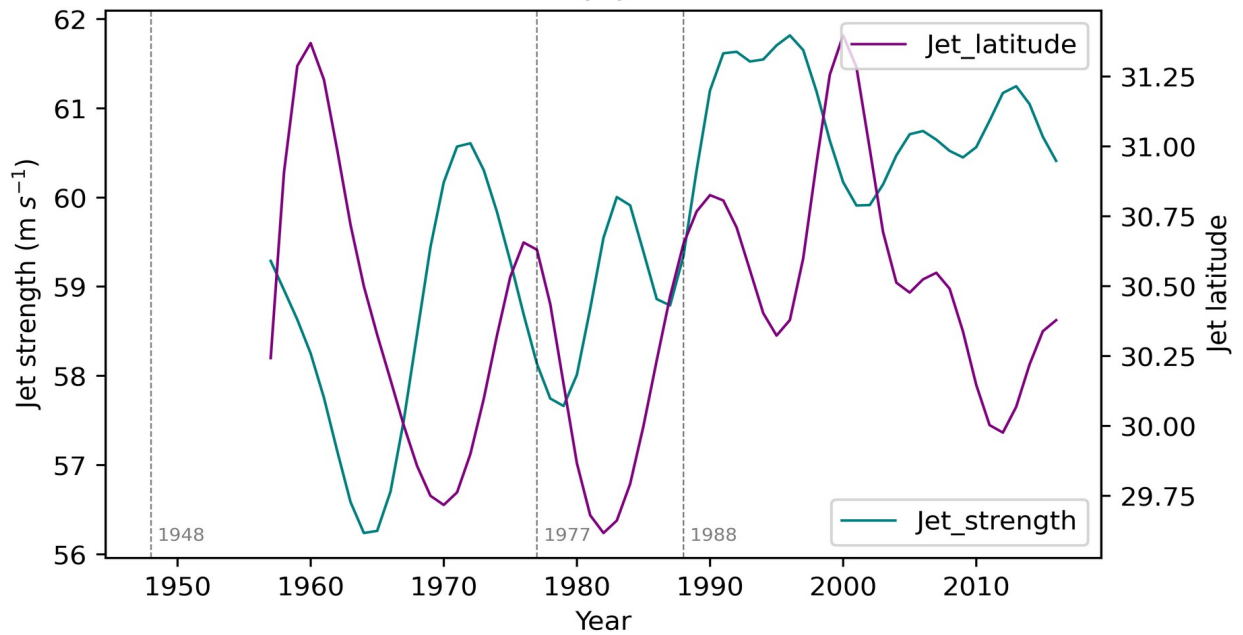
(a) PDO- minus PDO+



(b) PDO- minus PDO+



(c)



488 **Figure 5: Composite difference of (a) U-wind (colour; m/s), wind (vectors; m s⁻¹), and**
 489 **geopotential height (contours; m), (b) vertically averaged temperature (°C) from 300hPa to**
 490 **500hPa level during DJF between negative and positive epoch of PDO, (c) time series of 9-year**
 491 **filtered strength (red) and latitude (blue) of DJF subtropical westerly jet (STJ) over KH**
 492 **(green box; fig. 2) from 1940 to 2022.**

493

494

495

496

497

498

499

500

501

502

503

504

505

506

507

508

509

510

511

512

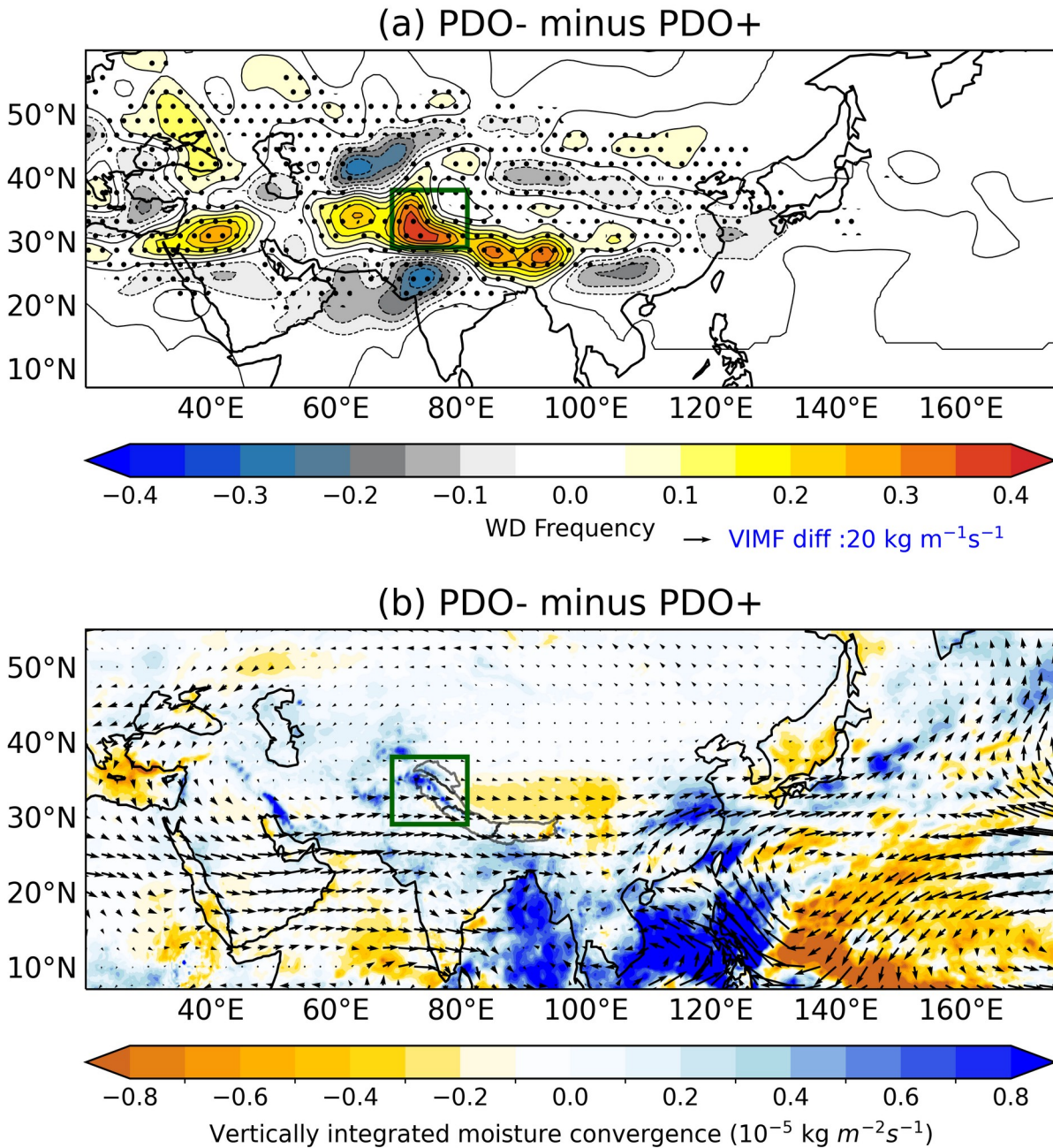
513

514

515

516

517



518 **Figure 6: Composite difference of (a) WD frequency, and (b) vertically integrated moisture**
 519 **flux (vectors; kg m⁻¹ s⁻¹) and vertically integrated moisture convergence (colours; kg m⁻² s⁻¹)**
 520 **during DJF between negative and positive epoch of PDO from 1940 to 2022. Stippling in (a)**

521 **indicates where the differences are significant at a 95% confidence level, as determined by the**
522 **two tailed Welch's t-test.**

523

524 **Author Contributions:**

525 **Priya Bharati:** conceptualization; formal analysis; methodology; investigation; software;
526 visualization; writing original draft. **Kieran M. R. Hunt:** conceptualization; methodology;
527 software; writing - review and editing. **Pranab Deb:** supervision; conceptualization; writing –
528 review and editing.

529 **Competing interests:** The contact author has declared that none of the authors has any
530 competing interests.

531 **Acknowledgements:**

532 The work is carried at CORAL, Indian Institute of Technology Kharagpur under supervision of
533 Pranab Deb. Priya Bharati is funded through the Ministry of Science and Technology, Government
534 of India, Council of Scientific and Industrial Research (CSIR; 09/081(1371)/2019-EMR-I). KMRH
535 is supported by a NERC Independent Research Fellowship (MITRE; NE/W007924/1).

536

537 **References:**

538 Adler, R., Sapiano, M., Huffman, G., Bolvin, D., Gu, G., Wang, J., and Becker, A.: The new version
539 2.3 of the Global Precipitation Climatology Project (GPCP) monthly analysis product, University of
540 Maryland, April, 1072-1084, 2016.

541

542 Aggarwal, D., Chakraborty R., and Attada, R.: Investigating bi-decadal precipitation changes over
543 the Northwest Himalayas during the pre-monsoon: role of Pacific decadal oscillations, *Climate*
544 *Dynamics*, 62(2), 1203-1218, 2024.

545

546 Archer, D. R., and Fowler, H. J.: Spatial and temporal variations in precipitation in the Upper Indus
547 Basin, global teleconnections and hydrological implications, *Hydrology and Earth System Sciences*,
548 8(1), 47-61, 2004.

549

550 Armstrong, R. L., Rittger, K., Brodzik, M. J., Racoviteanu, A., Barrett, A. P., Khalsa, S. J. S., and
551 Armstrong, B.: Runoff from glacier ice and seasonal snow in High Asia: separating melt water
552 sources in river flow, *Regional Environmental Change*, 19, 1249-1261, 2019.

553

554 Barlow, M., Wheeler, M., Lyon, B., and Cullen, H.: Modulation of daily precipitation over
555 southwest Asia by the Madden–Julian oscillation, *Monthly weather review*, 133(12), 3579-3594,
556 2005.

557

558 Basu, S., Bieniek, P. A., and Deoras, A.: An investigation of reduced western disturbance activity
559 over Northwest India in November-December 2015 compared to 2014-A case study, *Asia-Pacific*
560 *Journal of Atmospheric Sciences*, 53, 75-83, 2017.

561

562 Baudouin, J. P., Herzog, M., and Petrie, C. A.: Cross-validating precipitation datasets in the Indus
563 River basin, *Hydrology and Earth System Sciences*, 24(1), 427-450, 2020.

564

565 Beck, H., Pan, M., Roy, T., and Wood, E. F.: Evaluation of 27 precipitation datasets using Stage-IV
566 gauge-radar data for the CONUS, *AGU Fall Meeting 2018*, 2018.

567

568 Behera, S. K., and Yamagata, T.: Subtropical SST dipole events in the southern Indian Ocean,
569 *Geophysical Research Letters*, 28(2), 327-330, 2001.

570

571 Bharati, P., Deb, P., Hunt, K., Orr, A., and Dash, M. K.: ENSO-induced latitudinal variation of the
572 subtropical jet modulates extreme winter precipitation over the Western Himalaya, *Advances in*
573 *Atmospheric Sciences*, 10.1007/s00376-024-4057-2, 2024.

574

575 Bolch, T., Kulkarni, A., Käab, A., Huggel, C., Paul, F., Cogley, J. G., and Stoffel, M.: The state and
576 fate of Himalayan glaciers, *Science*, 336(6079), 310-314, 2012.

577

578 Bonekamp, P. N., De Kok, R. J., Collier, E., and Immerzeel, W. W.: Contrasting meteorological
579 drivers of the glacier mass balance between the Karakoram and central Himalaya, *Frontiers in Earth*
580 *Science*, 7, 107, 2019.

581

582 Bookhagen, B., and Burbank, D. W.: Toward a complete Himalayan hydrological budget:
583 Spatiotemporal distribution of snowmelt and rainfall and their impact on river discharge, *Journal of*
584 *Geophysical Research: Earth Surface*, 115(F3), 2010.

585

586 Bosilovich, M. G., Chen, J., Robertson, F. R., and Adler, R. F.: Evaluation of global precipitation in
587 reanalyses, *Journal of applied meteorology and climatology*, 47(9), 2279-2299, 2008.

588

589 Cannon, F., Carvalho, L. M., Jones, C., and Bookhagen, B.: Multi-annual variations in winter
590 westerly disturbance activity affecting the Himalaya, *Climate dynamics*, 44, 441-455, 2015.

591

592 Cannon, F., Carvalho, L. M., Jones, C., Hoell, A., Norris, J., Kiladis, G. N., and Tahir, A. A.: The
593 influence of tropical forcing on extreme winter precipitation in the western Himalaya, *Climate*
594 *Dynamics*, 48, 1213-1232, 2017.

595

596 Dahri, Z. H., Moors, E., Ludwig, F., Ahmad, S., Khan, A., Ali, I., and Kabat, P.: Adjustment of
597 measurement errors to reconcile precipitation distribution in the high-altitude Indus basin,
598 *International Journal of Climatology* 2018; 38: 3842–3860, 2018.

599

600 Dai, A. (2013). The influence of the inter-decadal Pacific oscillation on US precipitation during
601 1923–2010, *Climate dynamics*, 41(3), 633-646, 2013.

602

603 de Kok, R. J., Tuinenburg, O. A., Bonekamp, P. N., and Immerzeel, W. W.: Irrigation as a potential
604 driver for anomalous glacier behavior in High Mountain Asia, *Geophysical research letters*, 45(4),
605 2047-2054, 2018.

606

607 Deser, C., Phillips, A. S., & Hurrell, J. W.: Pacific interdecadal climate variability: Linkages
608 between the tropics and the North Pacific during boreal winter since 1900, *Journal of Climate*,
609 17(16), 3109-3124, 2004.

610

611 Dimri, A. P., Niyogi, D., Barros, A. P., Ridley, J., Mohanty, U. C., Yasunari, T., and Sikka, D. R.:
612 Western disturbances: a review, *Reviews of Geophysics*, 53(2), 225-246, 2015.

613

614 Dimri, A. P., and Dash, S. K.: Wintertime climatic trends in the western Himalayas, *Climatic*
615 *Change*, 111, 775-800, 2012.

616

617 Dimri, A. P., and Niyogi, D.: Regional climate model application at subgrid scale on Indian winter
618 monsoon over the western Himalayas, *International Journal of Climatology*, 33(9), 2013.

619

620 Dimri, A. P.: Relationship between ENSO phases with Northwest India winter precipitation,
621 *International Journal of Climatology*, 33(8), 1917-1923, 2013.

622

623 Dollan, I. J., Maina, F. Z., Kumar, S. V., Nikolopoulos, E. I., and Maggioni, V.: An assessment of
624 gridded precipitation products over High Mountain Asia, *Journal of Hydrology: Regional Studies*,
625 52, 101675, 2024.

626

627 Dong, B., and Dai, A.: The influence of the interdecadal Pacific oscillation on temperature and
628 precipitation over the globe, *Climate dynamics*, 45, 2667-2681, 2015.

629

630 Duchon, C. E.: Lanczos filtering in one and two dimensions, *Journal of Applied Meteorology and*
631 *Climatology*, 18(8), 1016-1022, 1979.

632

633 Enfield, D. B., Mestas-Nuñez, A. M., and Trimble, P. J.: The Atlantic multidecadal oscillation and
634 its relation to rainfall and river flows in the continental US, *Geophysical research letters*, 28(10),
635 2077-2080, 2001.

636

637 Farinotti, D., Immerzeel, W. W., de Kok, R. J., Quincey, D. J., and Dehecq, A.: Manifestations and
638 mechanisms of the Karakoram glacier Anomaly, *Nature geoscience*, 13(1), 8-16, 2020.

639

640 Filippi, L., Palazzi, E., von Hardenberg, J., and Provenzale, A.: Multidecadal variations in the
641 relationship between the NAO and winter precipitation in the Hindu Kush–Karakoram, *Journal of*
642 *climate*, 27(20), 7890-7902, 2014.

643

644 Forsythe, N., Fowler, H. J., Li, X. F., Blenkinsop, S., and Pritchard, D.: Karakoram temperature and
645 glacial melt driven by regional atmospheric circulation variability, *Nature Climate Change*, 7(9),
646 664-670, 2017.

647

648 Fowler, H. J., and Archer, D. R.: Conflicting signals of climatic change in the Upper Indus Basin,
649 *Journal of climate*, 19(17), 4276-4293, 2006.

650

651 Gardelle, J., Berthier, E., & Arnaud, Y.: Slight mass gain of Karakoram glaciers in the early twenty-
652 first century, *Nature geoscience*, 5(5), 322-325, 2012.

653

654 Gelaro, R., McCarty, W., Suárez, M. J., Todling, R., Molod, A., Takacs, L., and Zhao, B.: The
655 modern-era retrospective analysis for research and applications, version 2 (MERRA-2), *Journal of*
656 *climate*, 30(14), 5419-5454, 2017.

657

658 Harris, I. P. D. J., Jones, P., Osborn, T., and Lister, D.: Updated high-resolution grids of monthly
659 climatic observations-the CRU TS3. 10 Dataset, *International journal of climatology*, 34, 623-642,
660 2014.

661

662 Hersbach, H., de Rosnay, P., Bell, B., Schepers, D., Simmons, A., Soci, C., and Berrisford, P.:
663 Operational global reanalysis: Progress, future directions and synergies with NWP (ERA report
664 Series No. 27), European Centre for Medium Range Weather Forecasts: Reading, UK, 2018.
665

666 Hewitt, K.: The Karakoram anomaly? Glacier expansion and the elevation effect, Karakoram
667 Himalaya, Mountain Research and Development, 332-340, 2005.
668

669 Hewitt, K. (2014): Glaciers of the Karakoram Himalaya, Encyclopedia of Snow, Ice and Glaciers,
670 edited by: Singh, VP, Singh, P., and Haritashya, UK, Springer Netherlands, Dordrecht, 429-436,
671 2014.
672

673 Wester, Philippus, Mishra, Arabinda, Mukherji, Aditi, Shrestha, Arun Bhakta (Eds.): The Hindu
674 Kush Himalaya Assessment: Mountains, Climate Change, Sustainability and People, Springer,
675 HIMAP, 2020.
676

677 Hoell, A., Barlow, M., and Saini, R.: Intraseasonal and seasonal-to-interannual Indian Ocean
678 convection and hemispheric teleconnections, Journal of Climate, 26(22), 8850-8867, 2013.
679

680 Huffman, G. J., Bolvin, D. T., Nelkin, E. J., Wolff, D. B., Adler, R. F., Gu, G., and Stocker, E. F.:
681 The TRMM multisatellite precipitation analysis (TMPA): Quasi-global, multiyear, combined-sensor
682 precipitation estimates at fine scales, Journal of hydrometeorology, 8(1), 38-55, 2007.
683

684 Huffman, G. J., Bolvin, D. T., Braithwaite, D., Hsu, K., Joyce, R., Xie, P., and Yoo, S. H.: NASA
685 global precipitation measurement (GPM) integrated multi-satellite retrievals for GPM (IMERG),
686 Algorithm theoretical basis document (ATBD) version, 4(26), 2020-05, 2015.
687

688 Hunt, K. M., Turner, A. G., and Shaffrey, L. C.: The evolution, seasonality and impacts of western
689 disturbances, Quarterly Journal of the Royal Meteorological Society, 144(710), 278-290, 2018.
690

691 Hunt, K. M., and Fletcher, J. K.: The relationship between Indian monsoon rainfall and low-pressure
692 systems, *Climate Dynamics*, 53(3), 1859-1871, 2019.

693

694 Hu, X., and Yuan, W.: Evaluation of ERA5 precipitation over the eastern periphery of the Tibetan
695 plateau from the perspective of regional rainfall events, *International Journal of Climatology*, 41(4),
696 2625-2637, 2021.

697

698 Hunt, K. M., and Zaz, S. N.: Linking the North Atlantic Oscillation to winter precipitation over the
699 Western Himalaya through disturbances of the subtropical jet, *Climate Dynamics*, 60(7), 2389-
700 2403, 2023.

701

702 Hunt, K. M., Baudouin, J. P., Turner, A. G., Dimri, A. P., Jeelani, G., Pooja, and Palazzi, E.: Western
703 disturbances and climate variability: a review of recent developments, *EGU sphere*, 2024, 1-106,
704 2024.

705

706 Javed, A., Kumar, P., Hodges, K. I., Sein, D. V., Dubey, A. K., and Tiwari, G.: Does the recent
707 revival of western disturbances govern the Karakoram anomaly?, *Journal of Climate*, 35(13), 4383-
708 4402, 2022.

709

710 Joshi, M. K., Rai, A., and Pandey, A. C.: Validation of TMPA and GPCP 1DD against the ground
711 truth rain-gauge data for Indian region, *International journal of climatology*, 33(12), 2013.

712

713 Kääh, A., Berthier, E., Nuth, C., Gardelle, J., and Arnaud, Y.: Contrasting patterns of early twenty-
714 first-century glacier mass change in the Himalayas, *Nature*, 488(7412), 495-498, 2012.

715

716 Kamil, S., Almazroui, M., Kang, I. S., Hanif, M., Kucharski, F., Abid, M. A., and Saeed, F.: Long-
717 term ENSO relationship to precipitation and storm frequency over western Himalaya–Karakoram–
718 Hindukush region during the winter season, *Climate Dynamics*, 53, 5265-5278, 2019.

719

720 Kapnick, S. B., Delworth, T. L., Ashfaq, M., Malyshev, S., and Milly, P. C.: Snowfall less sensitive
721 to warming in Karakoram than in Himalayas due to a unique seasonal cycle, *Nature Geoscience*,
722 7(11), 834-840, 2014.

723

724 Kar, S. C., and Rana, S.: Interannual variability of winter precipitation over northwest India and
725 adjoining region: impact of global forcings, *Theoretical and applied climatology*, 116, 609-623,
726 2014.

727

728 Kishore, P., Jyothi, S., Basha, G., Rao, S. V. B., Rajeevan, M., Velicogna, I., and Sutterley, T. C.:
729 Precipitation climatology over India: validation with observations and reanalysis datasets and
730 spatial trends, *Climate dynamics*, 46, 541-556, 2016.

731

732 Krishnan, R., Sabin, T. P., Madhura, R. K., Vellore, R. K., Mujumdar, M., Sanjay, J., and Rajeevan,
733 M.: Non-monsoonal precipitation response over the Western Himalayas to climate change, *Climate*
734 *Dynamics*, 52, 4091-4109, 2019.

735

736 Krishnan, R., and Sugi, M.: Pacific decadal oscillation and variability of the Indian summer
737 monsoon rainfall, *Climate Dynamics*, 21, 233-242, 2003.

738

739 Krishnamurthy, L., and Krishnamurthy, V. J. C. D.: Influence of PDO on South Asian summer
740 monsoon and monsoon–ENSO relation, *Climate dynamics*, 42, 2397-2410, 2014.

741

742 Krishnamurthy, L., and Krishnamurthy, V.: Decadal scale oscillations and trend in the Indian
743 monsoon rainfall, *Climate dynamics*, 43, 319-331, 2014.

744

745 Lang, T. J., and Barros, A. P.: Winter storms in the central Himalayas, *Journal of the Meteorological*
746 *Society of Japan. Ser. II*, 82(3), 829-844, 2004.

747

748 Mantua, N. J., Hare, S. R., and Zhang, Y.: A Pacific interdecadal climate oscillation with impacts on
749 salmon production, *Oceanographic Literature Review*, 1(45), 36, 1998.

750

751 Ménégoz, M., Gallée, H., and Jacobi, H. W.: Precipitation and snow cover in the Himalaya: from
752 reanalysis to regional climate simulations, *Hydrology and Earth System Sciences*, 17(10), 3921-
753 3936, 2013.

754

755 Midhuna, T. M., and Dimri, A. P.: Impact of arctic oscillation on Indian winter monsoon,
756 *Meteorology and Atmospheric Physics*, 131, 1157-1167, 2019.

757

758 Midhuna, T. M., Kumar, P., and Dimri, A. P.: A new Western Disturbance Index for the Indian
759 winter monsoon, *Journal of Earth System Science*, 129, 1-14, 2020.

760

761 Newman, M., Shin, S. I., and Alexander, M. A. Natural variation in ENSO flavors, *Geophysical*
762 *Research Letters*, 38(14), 2011.

763

764 Newman, M., Alexander, M. A., Ault, T. R., Cobb, K. M., Deser, C., Di Lorenzo, E., and Smith, C.
765 A.: The Pacific decadal oscillation, revisited, *Journal of Climate*, 29(12), 4399-4427, 2016.

766

767 Nischal, Attada, R., and Hunt, K. M.: Evaluating winter precipitation over the western Himalayas in
768 a high-resolution Indian regional reanalysis using multisource climate datasets, *Journal of Applied*
769 *Meteorology and Climatology*, 61(11), 1613-1633, 2022.

770

771 Norris, J., Carvalho, L. M., Jones, C., and Cannon, F.: WRF simulations of two extreme snowfall
772 events associated with contrasting extratropical cyclones over the western and central Himalaya,
773 *Journal of Geophysical Research: Atmospheres*, 120(8), 3114-3138, 2015.

774

775 Norris, J., Carvalho, L. M., Jones, C., Cannon, F., Bookhagen, B., Palazzi, E., and Tahir, A. A.: The
776 spatiotemporal variability of precipitation over the Himalaya: evaluation of one-year WRF model
777 simulation, *Climate Dynamics*, 49, 2179-2204, 2017.

778

779 Norris, J., Carvalho, L. M., Jones, C., and Cannon, F.: Deciphering the contrasting climatic trends
780 between the central Himalaya and Karakoram with 36 years of WRF simulations, *Climate*
781 *Dynamics*, 52, 159-180, 2019.

782

783 Palazzi, E., Von Hardenberg, J., and Provenzale, A.: Precipitation in the Hindu-Kush Karakoram
784 Himalaya: observations and future scenarios, *Journal of Geophysical Research: Atmospheres*,
785 118(1), 85-100, 2013.

786

787 Power, S., Casey, T., Folland, C., Colman, A., and Mehta, V.: Inter-decadal modulation of the
788 impact of ENSO on Australia, *Climate dynamics*, 15, 319-324, 1999.

789

790 Pritchard, H. D.: Asia's shrinking glaciers protect large populations from drought stress, *Nature*,
791 569(7758), 649-654, 2019.

792

793 Qin, M., Li, D., Dai, A., Hua, W., and Ma, H.: The influence of the Pacific Decadal Oscillation on
794 North Central China precipitation during boreal autumn, *International Journal of Climatology*, 38,
795 e821-e831, 2018.

796

797 Rana, S., McGregor, J., and Renwick, J.: Precipitation seasonality over the Indian subcontinent: An
798 evaluation of gauge, reanalyses, and satellite retrievals, *Journal of Hydrometeorology*, 16(2), 631-
799 651, 2015.

800

801 Rana, S., McGregor, J., and Renwick, J.: Dominant modes of winter precipitation variability over
802 Central Southwest Asia and inter-decadal change in the ENSO teleconnection, *Climate dynamics*,
803 53, 5689-5707, 2019.

804

805 Ridley, J., Wiltshire, A., and Mathison, C.: More frequent occurrence of westerly disturbances in
806 Karakoram up to 2100, *Science of the Total Environment*, 468, S31-S35, 2013.

807

808 Schneider, U., Becker, A., Finger, P., Meyer-Christoffer, A. and Ziese, M.: GPCP full data monthly
809 product version 2018 at 0.25: monthly land-surface precipitation from rain-gauges built on GTS-
810 based and historical data, Global Precipitation Climatology Centre, 2018.

811

812 Singh, T., Saha, U., Prasad, V. S., and Gupta, M. D.: Assessment of newly-developed high
813 resolution reanalyses (IMDAA, NGFS and ERA5) against rainfall observations for Indian region,
814 *Atmospheric Research*, 259, 105679, 2021.

815

816 Syed, F. S., Giorgi, F., Pal, J. S., and Keay, K.: Regional climate model simulation of winter climate
817 over Central-Southwest Asia, with emphasis on NAO and ENSO effects, *International journal of*
818 *climatology*, 30(2), 220-235, 2010.

819

820 Tahir, A. A., Chevallier, P., Arnaud, Y., and Ahmad, B.: Snow cover dynamics and hydrological
821 regime of the Hunza River basin, Karakoram Range, Northern Pakistan, *Hydrology and Earth*
822 *System Sciences*, 15(7), 2275-2290, 2011.

823

824 Wang, L., Chen, W., Zhou, W., and Huang, R.: Interannual variations of East Asian trough axis at
825 500 hPa and its association with the East Asian winter monsoon pathway, *Journal of Climate*, 22(3),
826 600-614, 2009.

827

828 Wang, S., Huang, J., He, Y., and Guan, Y.: Combined effects of the Pacific decadal oscillation and
829 El Nino-southern oscillation on global land dry-wet changes, *Scientific reports*, 4(1), 6651, 2014.

830

831 Wang, W., Matthes, K., Omrani, N. E., and Latif, M.: Decadal variability of tropical tropopause
832 temperature and its relationship to the Pacific Decadal Oscillation, *Scientific reports*, 6(1), 29537,
833 2016.

834

835 Wang, X., Tolksdorf, V., Otto, M., and Scherer, D.: High Asia Refined Analysis Version 2 (HAR
836 v2): a New Atmospheric Data Set for the Third Pole Region, EGU General Assembly Conference
837 Abstracts (p. 8756), 2020.

838

839 Wittenberg, A. T., Rosati, A., Delworth, T. L., Vecchi, G. A., and Zeng, F.: ENSO modulation: Is it
840 decadal predictability?, *Journal of Climate*, 27(7), 2667-2681, 2014.

841

842 Wu, B., and Wang, J.: Winter Arctic oscillation, Siberian high and East Asian winter monsoon,
843 *Geophysical research letters*, 29(19), 3-1, 2002.

844

845 Wu, X., and Mao, J.: Interdecadal modulation of ENSO-related spring rainfall over South China by
846 the Pacific Decadal Oscillation, *Climate dynamics*, 47, 3203-3220, 2016.

847

848 Xie, P., and Arkin, P. A.: Global precipitation: A 17-year monthly analysis based on gauge
849 observations, satellite estimates, and numerical model outputs, *Bulletin of the American
850 meteorological society*, 78(11), 2539-2558, 1997.

851

852 Yadav, R. K., Rupa Kumar, K., and Rajeevan, M.: Increasing influence of ENSO and decreasing
853 influence of AO/NAO in the recent decades over northwest India winter precipitation, *Journal of
854 Geophysical Research: Atmospheres*, 114(D12), 2009.

855

856 Yadav, R. K., Yoo, J. H., Kucharski, F., and Abid, M. A.: Why is ENSO influencing northwest India
857 winter precipitation in recent decades?, *Journal of Climate*, 23(8), 1979-1993, 2010.

858

859 Yadav, R. K., Rupa Kumar, K., and Rajeevan, M.: Role of Indian Ocean sea surface temperatures in
860 modulating northwest Indian winter precipitation variability, *Theoretical and applied climatology*,
861 87, 73-83, 2007.

862

863 Yamagami, Y., and Tozuka, T.: Interdecadal changes of the Indian Ocean subtropical dipole mode,
864 *Climate Dynamics*, 44, 3057-3066, 2015.

865

866 Yang, Q., Ma, Z., and Xu, B.: Modulation of monthly precipitation patterns over East China by the
867 Pacific Decadal Oscillation, *Climatic change*, 144, 405-417, 2017.

868

869 Yatagai, A., Kamiguchi, K., Arakawa, O., Hamada, A., Yasutomi, N., and Kitoh, A.: APHRODITE;
870 Constructing a long-term daily gridded precipitation dataset for Asia based on a dense network of
871 rain gauges, *Bulletin of the American Meteorological Society*, 93(9), 1401-1415, 2012.

872

873 Yin, J., and Zhang, Y.: Decadal changes of East Asian jet streams and their relationship with the
874 mid-high latitude circulations, *Climate Dynamics*, 56, 2801-2821, 2021.

875

876 Yuan, X., Yang, K., Lu, H., He, J., Sun, J., and Wang, Y.: Characterizing the features of precipitation
877 for the Tibetan Plateau among four gridded datasets: Detection accuracy and spatio-temporal
878 variabilities, *Atmospheric Research*, 264, 105875, 2021.

879

880 Zhang, Y., Wallace, J. M., and Battisti, D. S.: ENSO-like interdecadal variability: 1900–93, *Journal*
881 *of climate*, 10(5), 1004-1020, 1997.

882

883 Zhang, R., and Delworth, T. L.: Impact of the Atlantic multidecadal oscillation on North Pacific
884 climate variability, *Geophysical Research Letters*, 34(23), 2007.